Monthly Notices
of the
ROYAL ASTRONOMICAL SOCIETY

Mon. Not. R. Astron. Soc. **410,** 1018–1026 (2011) doi:10.1111/j.1365-2966.2010.17498.x

Implications from the optical to ultraviolet flux ratio of Fe II emission in quasars

H. Sameshima,[1⋆] K. Kawara,[1] Y. Matsuoka,[2] S. Oyabu,[2] N. Asami[1] and N. Ienaka[1]

[1]*Institute of Astronomy, University of Tokyo, 2-21-1, Osawa, Mitaka, Tokyo 181-0015, Japan*
[2]*Graduate School of Science, Nagoya University, Furo-cho, Chikusa-ku, Nagoya 464-8602, Japan*

Accepted 2010 August 9. Received 2010 August 8; in original form 2010 March 4

Downloaded from https://academic.oup.com/mnras/article/410/2/1018/1030498 by guest on 18 April 2024

ABSTRACT

We investigate Fe II emission in the broad-line region (BLR) of active galactic nuclei by analysing the Fe II(UV), Fe II(λ4570) and Mg II emission lines in 884 quasars in the Sloan Digital Sky Survey Quasar catalogue in a redshift range of $0.727 < z < 0.804$. Fe II(λ4570)/Fe II(UV) is used to infer the column density of Fe II-emitting clouds and explore the excitation mechanism of Fe II emission lines. As suggested before in various works, the classical photoionization models fail to account for Fe II(λ4570)/Fe II(UV) by a factor of 10, which may suggest anisotropy of UV Fe II emission, or an alternative mechanism like shocks. The column density distribution derived from Fe II(λ4570)/Fe II(UV) indicates that radiation pressure plays an important role in BLR gas dynamics. We find a positive correlation between Fe II(λ4570)/Fe II(UV) and the Eddington ratio. We also find that the ionizing photon fraction must be much smaller than that previously suggested unless Fe II-emitting clouds are super-Eddington. Finally, we propose a physical interpretation of a striking set of correlations between various emission-line properties, known as 'Eigenvector 1'.

Key words: atomic processes – line: formation – radiation mechanisms: general – galaxies: active – galaxies: nuclei – quasars: emission lines.

1 INTRODUCTION

According to the models of nucleosynthesis, much of Fe comes from Type Ia supernovae (SNe Ia), while α elements such as O and Mg come from Type II supernovae (SNe II). Because of the difference in the lifetime of the progenitors, Fe enrichment delays relative to α elements. Hence, the abundance ratio of Fe to α elements [Fe/α] should have a sudden break at 1–2 Gyr after the initial burst of star formation [Hamann & Ferland 1993; Yoshii, Tsujimoto & Nomoto 1996; Yoshii, Tsujimoto & Kawara 1998; but see also recent studies, such as Matteucci et al. (2006); Totani et al. (2008), indicating a significant number of SNe Ia on relatively short time-scales]. Under the assumption that the Fe II/Mg II flux ratio reflects [Fe/Mg], various groups have measured Fe II/Mg II in high-redshift quasars hoping to discover such a break (e.g. Elston, Thompson & Hill 1994; Kawara et al. 1996; Dietrich et al. 2002, 2003; Iwamuro et al. 2002, 2004; Freudling, Corbin & Korista 2003; Maiolino et al. 2003; Kurk et al. 2007; Sameshima et al. 2009). However, these efforts have ended up with finding a large scatter of Fe II/Mg II showing little evolution.

A doubt is, thus, cast on the assumption that Fe II/Mg II reflects [Fe/Mg]. For example, Verner et al. (2003) suggested that Fe II/Mg II depends not only on the abundance but also on the microturbulence of Fe II-emitting clouds. Tsuzuki et al. (2006) showed that Fe II/Mg II correlates with the X-ray photon index, the full width at half-maximum (FWHM) of Mg II, the black hole mass, etc. For these reasons, prior to deriving the abundance from Fe II/Mg II, we must first clarify these non-abundance effects on the Fe II emission as well as the source of the Fe II excitation.

Column densities of clouds, which are considered to be one of the non-abundance factors largely affecting the Fe II emission, have lately attracted attention for their significances in determining whether or not the radiation pressure plays an important role in broad-line region (BLR) gas dynamics. Marconi et al. (2008) considered the effect of radiation pressure from ionizing photons on the estimation of the black hole mass, which is based on the application of the virial theorem to broad emission lines in active galactic nucleus (AGN) spectra, and suggested that the black hole mass can be severely underestimated if the effect of radiation pressure is ignored. Netzer (2009) then used the $M_{\rm BH}$–σ_* relation for a test of this suggestion, where $M_{\rm BH}$ is the black hole mass and σ_* is the velocity dispersion of host galaxies, concluding that radiation pressure effect is unimportant, while Marconi et al. (2009)

⋆E-mail: hsameshima@ioa.s.u-tokyo.ac.jp

© 2010 The Authors. 2010 The Author. Journal compilation © 2010 RAS

found the importance of radiation pressure by taking into account the intrinsic dispersion associated with the related parameters, in particular column densities of BLR clouds. However, there are no reliable column density estimates from observations up to date.

In this paper, we will estimate column densities of quasars selected from the Sloan Digital Sky Survey (SDSS) using Fe II, for investigating the excitation mechanism of Fe II emission and the BLR gas dynamics. In Section 2, we perform numerical calculations of Fe II emission lines to establish a method for estimating column densities. In Section 3, Fe II emission lines in the UV and optical as well as Mg II emission lines are measured in the SDSS quasars. The results and discussion about the Fe II emission mechanism, radiation pressure and the variety of quasar spectra called as 'Eigenvector 1' are given in Section 4. Throughout this paper, we assume a cosmology with $\Omega_{\rm m} = 0.3, \Omega_\Lambda = 0.7$ and $H_0 = 70\,{\rm km\,s^{-1}\,Mpc^{-1}}$.

2 METHODOLOGY

In the following, we use Fe II(UV) to denote the UV Fe II emission lines in $2000 < \lambda < 3000$ Å, Fe II(λ4570) to denote the optical Fe II emission lines in $4435 < \lambda < 4685$ Å and Mg II to denote the Mg II λ2798 emission line.

2.1 Fe II(λ4570)/Fe II(UV) to measure column densities

Fig. 1 shows a simplified Fe II Grotrian diagram. As can be seen, level 3–level 2 transitions give rise to optical Fe II emission lines such as the Fe II(λ4570) bump. A branching ratio of level 3–level 1 UV resonance transitions is significantly higher than that of level 3–level 2 optical transitions. Hence, strong optical Fe II emission requires a large optical depth between level 1 and level 3 such as $\tau_{13} > 10^3$ in order to transform the UV Fe II lines to optical Fe II lines through a large number of scatterings (cf. Collin & Joly 2000). Thus, the Fe II(λ4570)/Fe II(UV) flux ratio must strongly depend on τ_{13} and τ_{23}, which are the optical depths for photons emitted through level 3–level 1 and level 3–level 2 transitions, respectively. If so, the Fe II(λ4570)/Fe II(UV) can be an indicator of the column density.

Here, we use quite a simple model to indicate the dependence of Fe II(λ4570)/Fe II(UV) on the column density. First, we ignore level 4 shown in Fig. 1 and consider the Fe II as a three-level system.

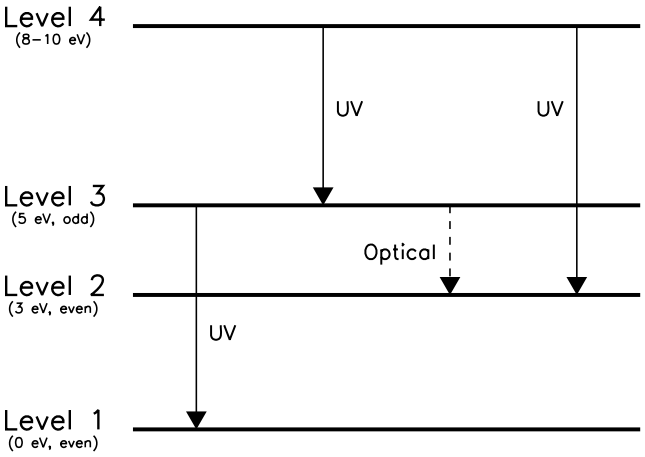

Figure 1. Simplified Fe II Grotrian diagram. Note that each level represents a large number of levels that have nearly the same excitation energies. The solid arrow indicates UV Fe II emission lines, while the dashed arrow indicates optical Fe II emission lines.

Secondly, we assume thermal equilibrium population between level 1 and level 2. Thirdly, we assume an expression of the local escape probability given by Netzer & Wills (1983) as $\epsilon_{ij} = (1 - \tau_{ij})/\tau_{ij}$. Although the model adopting these assumptions is obviously too oversimplified, it is useful to qualitatively understand how the line ratio depends on the physical parameters. The flux ratio is then written as

$$\frac{\text{Fe II}(\lambda4570)}{\text{Fe II(UV)}} \approx \frac{n_3 A_{32}\epsilon_{32} h\nu_{23}}{n_3 A_{31}\epsilon_{31} h\nu_{13}} \tag{1}$$

$$\propto \exp\left(\frac{2.9\ {\rm eV}}{kT}\right)\frac{1-{\rm e}^{-\tau_{23}}}{1-{\rm e}^{-\tau_{13}}}, \tag{2}$$

where n_3 is the population of level 3 and A_{ij} is the spontaneous emission rate from level i to level j. Following the fact that $\tau_{13} \gg 1$, the ratio can be roughly reduced to Fe II(λ4570)/Fe II(UV) $\propto 1 - {\rm e}^{-\tau_{23}}$. Since τ_{23} is proportional to the column density, the ratio is an increasing function of the column density. We will further discuss this matter in the following.

2.2 Photoionization models in the LOC scenario

Here we will show more sophisticated model calculations of Fe II(λ4570)/Fe II(UV). We performed photoionization model calculations with version C06.02 of the spectral simulation code CLOUDY, last described by Ferland et al. (1998), combined with a 371-level Fe^+ model (up to ~11.6 eV; Verner et al. 1999). The incident continuum is defined as

$$f_\nu \propto \nu^{\alpha_{\rm UV}} \exp(-h\nu/kT_{\rm BB}) \exp(-kT_{\rm IR}/h\nu) + a\nu^{\alpha_{\rm X}}. \tag{3}$$

The first term on the right-hand side of equation (3) expresses an accretion disc component, which is usually called *Big Bump*. $kT_{\rm BB}$ and $kT_{\rm IR}$ indicate the higher and the lower cut-off energies, respectively. The second term expresses a power-law X-ray component, which is set to zero below 1.36 eV while falls off as ν^{-3} above 100 keV. The coefficient a is set to produce the optical to X-ray spectral index $\alpha_{\rm ox}$.[1] We set these parameters to $(\alpha_{\rm UV}, \alpha_{\rm X}, \alpha_{\rm ox}, T_{\rm BB}, kT_{\rm IR}) = (-0.2, -1.8, -1.4, 1.5 \times 10^5\,{\rm K}, 0.136\,{\rm eV})$, which are adopted in Tsuzuki et al. (2006). This incident continuum illuminates a single cloud with hydrogen density $n_{\rm H}$, ionization parameter $U(\equiv \Phi/n_{\rm H}\,c$, where Φ is the ionizing photon flux and c is the velocity of light), column density $N_{\rm H}$ and solar abundance. We calculated the models in a range of $N_{\rm H} = 10^{21}$–10^{25} cm^{-2}, $n_{\rm H} = 10^7$–10^{14} cm^3 and $U = 10^{-5}$–10^0.

In the locally optimally emitting cloud (LOC) model (Baldwin et al. 1995), each line is emitted from clouds with a wide range of gas hydrogen densities and distances from the central continuum source, and the observed spectra are reproduced by integrating these clouds with an appropriate covering fraction distribution. The observed emission-line flux is, then, expressed as

$$L_{\rm line} \propto \int\int r^2 F(r, n_{\rm H}) f(r) g(n_{\rm H}) {\rm d}n_{\rm H} {\rm d}r, \tag{4}$$

where $F(r, n_{\rm H})$ is the emission-line flux of a single cloud at a distance r from the central continuum source and with $n_{\rm H}$, $f(r)$ is a cloud covering fraction with distance r and $g(n_{\rm H})$ is a fraction of clouds with $n_{\rm H}$. Matsuoka et al. (2007) showed that O I and Ca II emission lines in quasars, which are likely to emerge from the same gas as the Fe II emission lines, are well reproduced by an LOC

[1]The optical to X-ray spectral index $\alpha_{\rm ox}$ is defined as $f_\nu(2\ {\rm keV})/f_\nu(2500\ {\text Å}) = 403.3^{\alpha_{\rm ox}}$.

Downloaded from https://academic.oup.com/mnras/article/410/2/1018/1030498 by guest on 18 April 2024

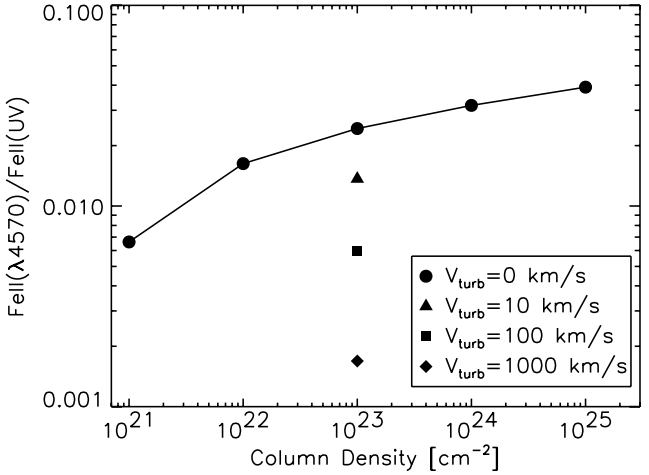

Figure 2. Fe II(λ4570)/Fe II(UV) versus column densities based on the photoionization models. $V_{\rm turb}$ is the microturbulence velocity of clouds. Note that, in the LOC, the calculation results are not dependent on $n_{\rm H}$ and U since clouds with different hydrogen densities and distances from the central continuum source are all integrated.

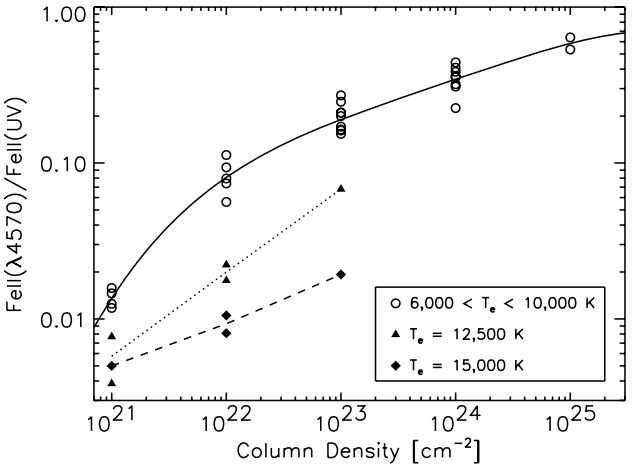

Figure 3. Fe II(λ4570)/Fe II(UV) versus column densities based on the collisionally ionized models taken from Joly (1987). The density ranges from 10^{10} to 10^{12} cm^{-3} and the column density from 10^{21} to 10^{25} cm^{-2}. Circles indicate the models with $6\,000 < T_{\rm e} < 10\,000$ K, triangles with $T_{\rm e} = 12\,500$ K and diamonds with $T_{\rm e} = 15\,000$ K. The solid line indicates the fitted fourth-order polynomial for samples with $6000 < T_{\rm e} < 10\,000$ K. The dotted and the dashed lines connect the median values of Fe II(λ4570)/Fe II(UV) at each column density for samples with $T_{\rm e} = 12\,500$ K and $T_{\rm e} = 15\,000$ K, respectively.

model with $f(r) \propto r^{-1}$ and $g(n_{\rm H}) \propto n_{\rm H}^{-1}$; hence, we have adopted these covering distributions. Baldwin et al. (1995) suggested that since clouds at large distances from the continuum source will form graphite grains which heavily suppress the line emissivity, clouds with $\Phi < 10^{18}$ s^{-1} cm^{-2} must be excluded from integration. Thus, we have calculated equation (4) for clouds which correspond to $\Phi \geq 10^{18}$ s^{-1} cm^{-2}.

Fig. 2 illustrates Fe II(λ4570)/Fe II(UV) as a function of the column density for photoionized clouds. Fe II(λ4570)/Fe II(UV) increases as the column density increases. It also shows that Fe II(λ4570)/Fe II(UV) decreases as the microturbulent velocity increases, consistent with Verner et al. (2003), and that Fe II(λ4570)/Fe II(UV) is maximum when no microturbulence is assumed to exist. This is explained as follows. Increasing microturbulent velocities broadens the line absorption profile, resulting in enhancement of the continuum photoexcitation. This effect is relatively large for high energy levels where the collisional excitation is inefficient for their high excitation potential. Thus, large microturbulent velocities relatively enhance the continuum photoexcitation to level 4 shown in Fig. 1, leading to emit more fluxes in the UV Fe II emission lines, thus decreasing Fe II(λ4570)/Fe II(UV). For photoionized clouds, Fe II(λ4570)/Fe II(UV) can be used as a column density indicator unless microturbulent velocities vary much from cloud to cloud.

It is noted that calculations adopting the other shapes of the incident continuum[2] show little changes for Fe II(λ4570)/Fe II(UV), indicating little dependence on the spectral energy distribution (SED) of the ionizing continuum.

2.3 Collisionally ionized models

As an alternative to photoionization models, we consider models in which a cloud is assumed to be in collisional equilibrium at a given electron temperature $T_{\rm e}$ and call them *collisionally ionized models*.

[2] Two types of SED given by Nagao, Murayama & Taniguchi (2001) are adopted. One is set to reproduce the ordinary SED of broad-line Seyfert 1 galaxies and the other is set to reproduce that of narrow-line Seyfert 1 galaxies.

In these models, the specific heating mechanism is not accounted for and arbitrary electron temperatures are given. It is noted that Fe II is collisionally excited in either mechanically heated clouds, such as through shocks, or photoionized clouds. In the latter case, the heating mechanism is specified to be the heating of the incident UV and X-ray photons.

Joly (1987) offers collisionally ionized model calculations. In her models, Fe II is approximated by a 14-level atom (up to ∼5.7 eV), and the emission region is assumed to be a homogeneous slab with constant hydrogen density $n_{\rm H}$, column density $N_{\rm H}$ and electron temperature $T_{\rm e}$ and assumed to not receive any external radiation. The electron temperature ranges from 6000 to 15 000 K, the density from 10^{10} to 10^{12} cm^{-3} and the column density from 10^{21} to 10^{25} cm^{-2}.

Fig. 3 shows Fe II(λ4570)/Fe II(UV) as a function of the column density, taken from Joly (1987). As expected from equation (2), it can be seen that Fe II(λ4570)/Fe II(UV) increases with the column density while it decreases with temperature. However, Fig. 3 shows that Fe II(λ4570)/Fe II(UV) does not much depend on temperature for $6000 < T_{\rm e} < 10\,000$ K. It is noted that Collin et al. (1980) and Joly (1987) showed that emission-line ratios including Fe II in quasars are well accounted for by cold clouds with $6000 < T_{\rm e} < 10\,000$ K. Thus, it is reasonable to assume that Fe II-emitting clouds have the temperatures in a range of $6000 < T_{\rm e} < 10\,000$ K, and Fe II(λ4570)/Fe II(UV) depends little on the temperature while strongly varies with the column density. We fit the data of $6000 < T_{\rm e} < 10\,000$ K models by a fourth-order polynomial and find

$$y = -0.72 + 0.28x - 0.046x^2 + 0.031x^3 - 0.0089x^4, \quad (5)$$

where $y = \log$Fe II(λ4570)/Fe II(UV) and $x = \log N_{\rm H}({\rm cm}^{-2}) - 23$. We will use this relation to estimate the column density of quasars.

Downloaded from https://academic.oup.com/mnras/article/410/2/1018/1030498 by guest on 18 April 2024

3 ANALYSIS OF QUASAR SPECTRA

3.1 Sample selection

We have analysed quasar spectra selected from the fourth edition of the SDSS Quasar catalogue (Schneider et al. 2007). SDSS uses a dedicated 2.5-m telescope at the Apache Point Observatory equipped with a CCD camera to image the sky in five optical bands and two digital spectrographs, one covering a wavelength range from 3800 to 6150 Å and the other from 5800 to 9200 Å. The spectral resolution ranges from 1850 to 2200. The fourth edition of the SDSS Quasar catalogue consists of the objects in the Fifth Data Release and contains 77 429 quasars.

In order to measure the Fe II(UV) and Fe II(λ4570) emission lines simultaneously, we have selected spectra which cover the wavelength range from 2200 to 5100 Å in the rest frame, corresponding to the redshift range from 0.727 to 0.804. 2189 objects meet this requirement. We then checked the signal-to-noise ratio (S/N) per pixel for each spectrum which fulfils median S/N > 10 per pixel at their continuum levels for accurate flux measurements. 946 objects meet this requirement. All the spectra were inspected by eyes and 62 spectra were rejected because of wavelength discontinuity, terrible contamination by host galaxy star light, etc. Our final sample thus consists of 884 spectra.

Prior to the measurements, the quasar spectra were dereddened for the Galactic extinction according to the dust map by Schlegel, Finkbeiner & Davis (1998) using the Milky Way extinction curve by Pei (1992).

Since SDSS quasars are flux-limited in the survey, low-luminosity quasars are lost in the SDSS sample. Fig. 4 shows luminosity versus redshift for our sample. Because of the narrow redshift coverage for our sample, the minimum luminosity is almost constant and roughly estimated to be $\lambda L_{5100} = 10^{44.7}$ erg s^{-1}.

3.2 Continuum and line fitting

In the UV to optical, the quasar continuum is composed of (i) the power-law continuum $F_\lambda^{\rm PL}$, (ii) the Balmer continuum $F_\lambda^{\rm BaC}$ and (iii) the Fe II pseudo-continuum $F_\lambda^{\rm Fe\,II}$. Thus, we assumed the following formula as a model continuum $F_\lambda^{\rm cont}$:

$$F_\lambda^{\rm cont} = F_\lambda^{\rm PL} + F_\lambda^{\rm BaC} + F_\lambda^{\rm Fe\,II}. \quad (6)$$

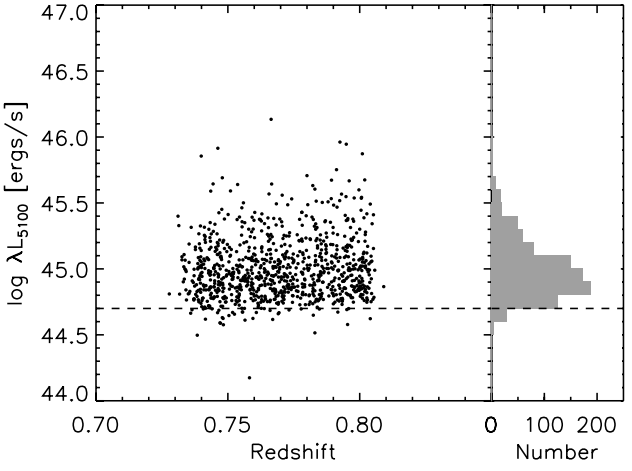

Figure 4. Luminosity λL_{5100} versus redshift for our sample. Luminosity distribution is also displayed in the right-hand panel. The dashed line shows a rough estimate of the minimum quasar luminosity for our sample.

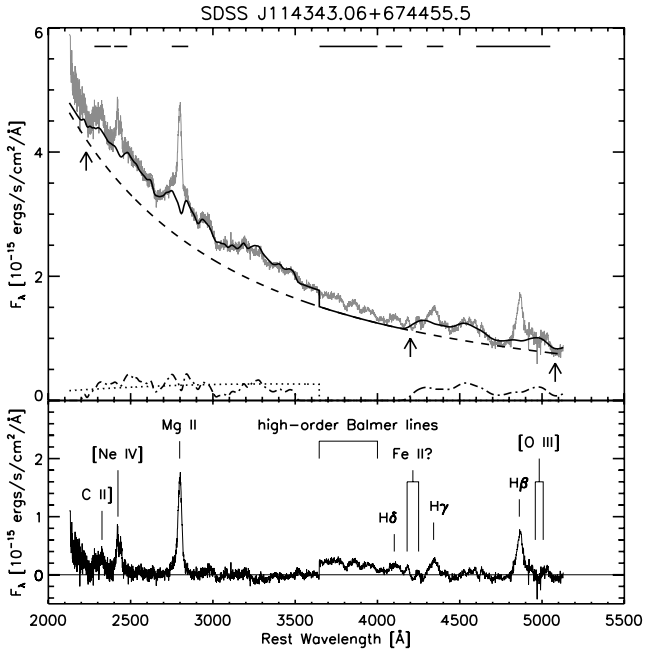

Figure 5. Top: sample quasar spectrum (grey line) with the fitted power-law continuum $F_\lambda^{\rm PL}$ (dashed line), the Balmer continuum $F_\lambda^{\rm BaC}$ (dotted line), the Fe II pseudo-continuum $F_\lambda^{\rm Fe\,II}$ (dot–dashed line) and the sum of the three continua $F_\lambda^{\rm cont}$ (solid line). Arrows indicate the continuum windows adopted in the power-low continuum fitting. Horizontal thick bars indicate the masked region adopted in the Fe II pseudo-continuum fitting. Bottom: the continuum-subtracted spectrum.

3.2.1 *Power-law continuum*

The power-law continuum is simply written as follows:

$$F_\lambda^{\rm PL} = F_{5100}\left(\frac{\lambda}{5100}\right)^{\alpha}. \quad (7)$$

The free parameters of this model are a scaling factor F_{5100} and a power-law index α. We chose three fitting ranges, 2200–2230, 4180–4220 and 5050–5100 Å, respectively, as continuum windows, since these areas have little emission lines (see Fig. 5). There are, however, the Balmer continuum and the Fe II pseudo-continuum underneath these regions, requiring some corrections.

Tsuzuki et al. (2006) gave 14 quasar spectra covering a wide wavelength range and measured accurately their continuum levels. We fitted power-law continuum models to their spectra in the continuum windows and compared the continuum levels with those given by them. We found that our method systematically overestimates the continuum levels, 10.1 per cent at 2200–2230 Å, 5.7 per cent at 4180–4220 Å and 3.4 per cent at 5050–5100 Å. According to these results, we first reduced the flux densities of the object by these amounts at each continuum window and then fitted the power-law continuum. An example of the fitted power-law continuum is indicated by a dashed line in Fig. 5. The measurement error of the continuum levels is estimated to be less than 10 per cent.

3.2.2 *Balmer continuum*

Grandi (1982) gives a formula describing the Balmer continuum produced by a uniform temperature, partially optically thick

Downloaded from https://academic.oup.com/mnras/article/410/2/1018/1030498 by guest on 18 April 2024

cloud:

$$F_{\lambda}^{\rm BaC} = F_{\rm BaC} B_{\lambda}(T_{\rm e}) \left[1 - \exp \left\{ -\tau_{\rm BE} \left(\frac{\lambda}{\lambda_{\rm BE}} \right)^3 \right\} \right], \quad (8)$$

where $B_{\lambda}(T_{\rm e})$ is the Planck function at the electron temperature $T_{\rm e}$ and $\tau_{\rm BE}$ is the optical depth at the Balmer edge at $\lambda = 3646$ Å. Kurk et al. (2007) assumed gas clouds of uniform temperature ($T_{\rm e} = 15\,000$ K) and the optical depth fixed to $\tau_{\rm BE} = 1$, and fitted equation (8) to their sample quasar spectra to estimate the strength of the Balmer continuum (see also Dietrich et al. 2003). We followed their method and assumed $T_{\rm e} = 15\,000$ K and $\tau_{\rm BE} = 1$. Only one parameter, namely the scalefactor $F_{\rm BaC}$, is set free and is decided by fitting equation (8) to the power-law-subtracted spectrum at 3600–3645 Å. An example of the fitted Balmer continuum is indicated by a dotted line in Fig. 5.

3.2.3 *Fe II pseudo-continuum*

Since Fe II has enormous energy levels, neighbouring emission lines contaminate heavily with each other, which makes it difficult to measure the Fe II emission lines. One approach to measuring the Fe II emission lines is to use Fe II templates. So far, several Fe II templates are derived from the narrow-line Seyfert 1 galaxy, I Zw 1.

In the UV, Vestergaard & Wilkes (2001) and Tsuzuki et al. (2006) give their Fe II templates. The template given by Vestergaard & Wilkes (2001) does not cover around the Mg II line. Tsuzuki et al. (2006) used a synthetic spectrum calculated with the CLOUDY photoionization code in order to separate the Fe II emission from the Mg II line and derived semi-empirically the Fe II template which covers around the Mg II line. Since we want to measure the Mg II emission line, we decided to use the UV Fe II template given by Tsuzuki et al. (2006).

In the optical, Véron-Cetty, Joly & Véron (2004) and Tsuzuki et al. (2006) open their Fe II templates to the public. Véron-Cetty et al. (2004) carefully analysed the Fe II emission lines in I Zw 1, finding that the Fe II lines are emitted from both BLR and narrow-line region (NLR). They succeeded to separate them and called the broad-line system L1 and the narrow-line system N3. Tsuzuki et al. (2006) also analysed the spectrum of I Zw 1 and derived the optical Fe II template, which was however not separated into the BLR and the NLR components. We applied both the broad-line system L1 template given by Véron-Cetty et al. (2004) and the optical Fe II template given by Tsuzuki et al. (2006) to all of our samples, finding that the latter has a slightly smaller average χ^2_{ν} value [median $\chi^2_{\nu} \sim 1.48$ for Tsuzuki et al. (2006), while median $\chi^2_{\nu} \sim 1.58$ for Véron-Cetty et al. (2004)]. Here we use the optical Fe II template given by Tsuzuki et al. (2006).

Prior to applying the Fe II template to each quasar, broadening of the template spectrum is needed. Thus, we modelled the Fe II flux density as follows:

$$F_{\lambda}^{\rm Fe\,II}(x) = F_{\rm Fe\,II} \int_{-\infty}^{\infty} F_{\lambda}^{\rm template}(x') \times \exp \left[-\frac{4c^2 \ln 2 (x - x')^2}{{\rm FWHM_{conv}}^2} \right] {\rm d}x', \quad (9)$$

where $x \equiv \ln \lambda$, c is the velocity of light and $\rm FWHM_{conv}$ represents the FWHM of the convolved Gauss function. We first calculated equation (9) with $\rm FWHM_{conv}$ in a range of $\rm FWHM_{conv} = 0$–5000 km s^{-1} stepped by 100 km s^{-1}, thus prepared 51 Fe II emission-line models. Then we flux-scaled each model to fit the continuum-subtracted spectrum (i.e. the spectrum after subtracting the power law and the Balmer continuum) and adopted the model which gives the smallest χ^2_{ν} value. We decided mask regions as follows: 2280–2380 Å for C II] λ2326, 2400–2480 Å for [Ne IV] λ2423 and Fe III, 2750–2850 Å for Mg II, 3647–4000 Å for high-order Balmer lines, 4050–4150 Å for Hδ, 4300–4400 Å for Hγ and 4600–5050 Å for He II λ4686, Hβ and [O III] λλ4959,5009. An example of the fitted Fe II pseudo-continuum is indicated by a dot–dashed line in Fig. 5.

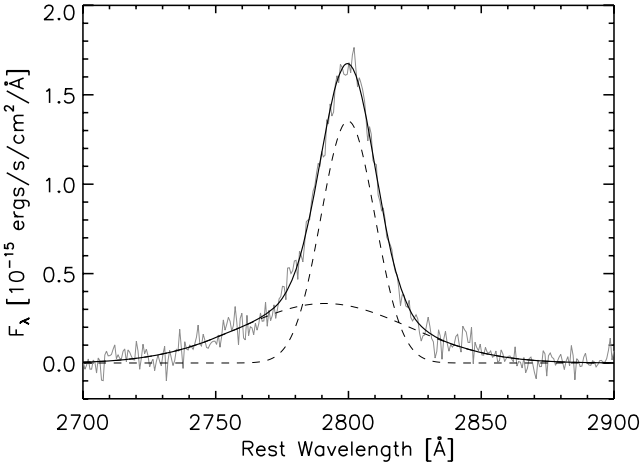

Figure 6. Mg II emission line (grey line) with fitted two Gaussian components (dashed lines) and the sum of the two Gaussians (solid line).

3.2.4 *Mg II lines*

After subtracting the continuum components, we have measured the Mg II emission line for estimating the black hole mass from its FWHM. We have fitted the Mg II emission-line profile by two Gaussian components. Fig. 6 shows an example of the Mg II emission-line fitting.

3.3 Black hole mass and Eddington luminosity

For the classical black hole mass estimate in which the radiation pressure effect is neglected, we use the following formula given by McLure & Jarvis (2002):

$$M_{\rm BH,0} = 3.37 \left(\frac{\lambda L_{3000}}{10^{37}\ {\rm W}} \right)^{0.47} \left[\frac{\rm FWHM(Mg\,II)}{\rm km\ s^{-1}} \right]^2 {\rm M}_{\odot} \quad (10)$$

The classical Eddington luminosity is given as follows:

$$L_{\rm Edd,0} = \frac{4\pi c G M_{\rm BH,0} m_{\rm p}}{\sigma_{\rm T}} \sim 1.26 \times 10^{38} \frac{M_{\rm BH,0}}{{\rm M}_{\odot}}\ ({\rm erg\ s^{-1}}), \quad (11)$$

where c is the velocity of light, $m_{\rm p}$ is the proton mass and $\sigma_{\rm T}$ is the Thomson cross-section.

On the other hand, Marconi et al. (2008) suggested that the force of the radiation pressure should be corrected to derive the black hole mass. They give the radiation-pressure-corrected black hole mass $M_{\rm BH,rad}$ and Eddington luminosity $L_{\rm Edd,rad}$ as follows:

$$M_{\rm BH,rad} = M_{\rm BH,0} + \frac{L_{\rm bol}}{L_{\rm Edd,0}} \left(1 - a + \frac{a}{\sigma_{\rm T} N_{\rm H}} \right) M_{\rm BH,0} \quad (12)$$

$$L_{\rm Edd,rad} = \frac{L_{\rm Edd,0}}{1 - a + a/(\sigma_{\rm T} N_{\rm H})} \quad (13)$$

$$a \equiv \frac{L_{\rm ion}}{L_{\rm bol}}, \quad (14)$$

Downloaded from https://academic.oup.com/mnras/article/410/2/1018/1030498 by guest on 18 April 2024

where $L_{\rm bol}$ is the bolometric luminosity, $L_{\rm ion}$ is the total luminosity of the ionizing continuum (i.e. $h\nu > 13.6$ eV) and a is the ionizing photon fraction. The second term on the right-hand side of equation (12) represents the correction term of the radiation pressure. We here adopt a bolometric correction $L_{\rm bol} = 9\lambda L_{5100}$ given by Kaspi et al. (2000).

3.4 Error estimate

We performed a Monte Carlo simulation similar to that done in Hu et al. (2008) for estimating the measurement errors. The detail of the procedure is as follows.

(i) *Generating a composite spectrum*. Following Vanden Berk et al. (2001), we generated a composite spectrum using all of our samples. This composite spectrum represents a typical quasar spectrum for our samples.

(ii) *Obtaining typical emission-line profiles*. We applied the measurement methods written in Section 3.2 to the composite spectrum and obtained typical emission-line profiles for Fe II(UV), Fe II(λ4570) and Mg II.

(iii) *Making artificial spectra*. We combined these line profiles with the power-law continuum and the Balmer continuum. Thus, the simulated spectrum is written as follows:

$$\begin{aligned} F_\lambda^{\rm sim} = {} & F_\lambda^{\rm PL}(F_{5100}, \alpha) + F_\lambda^{\rm BaC}(F_{\rm BaC}) \\ & + F_\lambda^{{\rm Fe\,II_{UV}}}(EW_{\rm Fe\,II_{UV}}) \\ & + F_\lambda^{{\rm Fe\,II}_{\lambda4570}}(EW_{{\rm Fe\,II}_{\lambda4570}}) \\ & + F_\lambda^{\rm Mg\,II}(EW_{\rm Mg\,II}, FWHM_{\rm Mg\,II}). \end{aligned} \quad (15)$$

Note that, for simplicity, we ignored the broadening of the pseudo-Fe II continuum. Values of input parameters, which are given in the parentheses in equation (15), are randomly sampled from probability distributions that are made to reflect the observations. Thus, we generated 1000 simulated spectra.

(iv) *Generating a noise template*. Using all the noise spectra produced by the SDSS pipeline for our samples, we generated a composite spectrum following Vanden Berk et al. (2001) and named it a noise template. This noise template is scaled so that the resulting median S/N is 10 per pixel at the continuum level for each simulated spectrum, and is treated as its noise.

Now we have the 1000 simulated spectra with their noise. The measurement methods written in Section 3.2 are applied to these simulated spectra. We calculate the value $\delta_{\rm sim} = (P_{\rm out} - P_{\rm in})/P_{\rm in}$ for each simulated spectrum, where $P_{\rm in}$ represents the input parameters (i.e. the values given in the parentheses in equation 15) and $P_{\rm out}$ represents the corresponding measured values for the simulated spectra. We consider $\sigma_{\rm sim}$, a standard deviation of $\delta_{\rm sim}$, as 1σ error of the measurement. Thus, we evaluate the measurement errors to be 16.4 per cent for equivalent width (EW) of Fe II(UV), 22.9 per cent for EW of Fe II(λ4570) and 7.9 per cent for FWHM(Mg II). The simulation implies the measurement error to be 2.9 per cent for the luminosity, which is less than 10 per cent estimated in the power-law fitting. Therefore, we decided to evaluate the measurement error to be 10 per cent for λL_{3000} and λL_{5100}.

4 RESULTS AND DISCUSSION

4.1 On the excitation mechanism of Fe II emission

Fig. 7 shows the observed Fe II(λ4570)/Fe II(UV) distribution. As can be seen from the comparison between Fig. 7 and Fig. 2, our

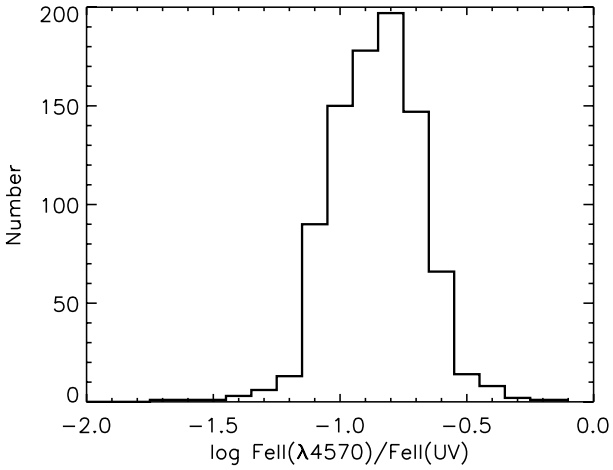

Figure 7. Observed Fe II(λ4570)/Fe II(UV) flux ratio distribution. The average of log Fe II(λ4570)/Fe II(UV) is −0.8 and the standard deviation is 0.2 dex, in disagreement with the range that the photoionization models predict.

photoionization models underpredict the Fe II(λ4570)/Fe II(UV) by a factor of 10, failing to account for the observations. This result is consistent with the preceding study by Baldwin et al. (2004). Additional microturbulence to the photoionized clouds makes the situation even worse. Thus, Fig. 7 seems to challenge classical photoionized pictures of Fe II-emitting clouds. On the other hand, in the case of the collisionally ionized models shown in Fig. 3, the observed Fe II(λ4570)/Fe II(UV) flux ratios are well reproduced with $10^{22} < N_{\rm H} < 10^{24}$ cm^{-2} and $6000 < T_{\rm e} < 10\,000$ K.

These results give two remarks: (1) the Fe II-emitting clouds in quasars are heated to $6000 < T_{\rm e} < 10\,000$ K and (2) the UV and the X-ray photons, which are the heating source in our photoionization models, fail to heat the gas to such temperatures (probably heat the gas too hot!). One possible interpretation is that the Fe II-emitting clouds are heated by an alternative mechanism such as through shocks. Here we note that there is a reverberation mapping study implying shock heating for Fe II emission. Kuehn et al. (2008) analysed optical Fe II emission bands in Ark 120, finding that they do not respond to the continuum variation. Thus, the optical Fe II-emitting region may be heated by other mechanisms than photoionization. These results favour the shock heating for the optical Fe II-emitting region, but there are also difficulties. First, the amount of shock-processed matter would probably be too large. Secondly, as Kuehn et al. (2008) showed, collisionally ionized models failed to match the shape of the optical Fe II emission band. Thirdly, the fact that there is no response to the continuum variation for optical Fe II emission bands can also be interpreted as that the emitting region is too large to vary optical Fe II emission in observable time-scales. Unless shocks are a viable solution, the failure of the photoionization model simply indicates that it is not predicting the correct heating rate or that the radiative transport calculations are not correct.

One possible cause disturbing classical photoionization models to reproduce the observations may be the assumption that the Fe II emission is isotropic. Ferland et al. (2009) recently suggested that UV Fe II lines are beamed towards a central source while optical Fe II lines are emitted isotropically. Then photoionization models can reproduce the observed UV to optical Fe II flux ratio if the Fe II-emitting clouds are distributed asymmetrically so that we mainly observe their shielded faces. However, this needs special geometrical distributions like Type II AGNs, a thick Fe II-emitting gas surrounding the central source with a substantial covering factor

Downloaded from https://academic.oup.com/mnras/article/410/2/1018/1030498 by guest on 18 April 2024

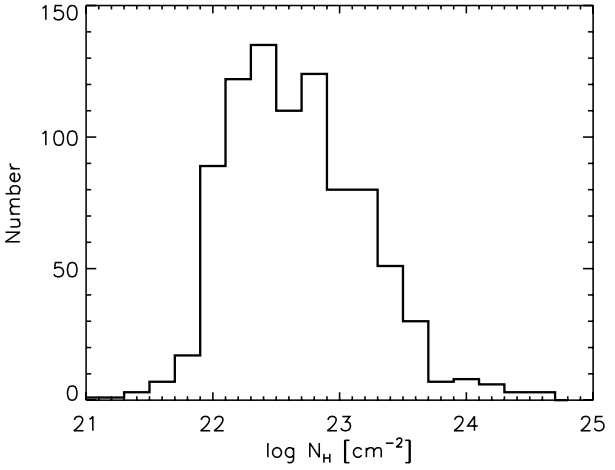

Figure 8. Estimated column density distribution. The average and the standard deviation of the distribution are $(\overline{\log N_{\rm H}}, \sigma_{\log N_{\rm H}}) = (22.8, 0.5)$, providing observational support for the assumption adopted in Marconi et al. (2009).

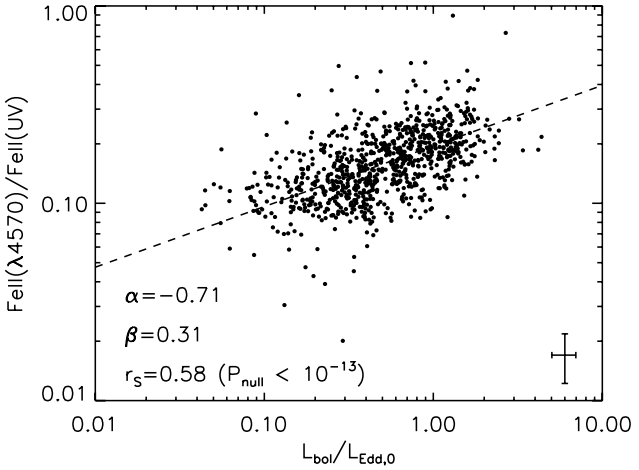

Figure 9. Eddington ratio versus Fe II(λ4570)/Fe II(UV) flux ratio. A typical 1σ error is indicated at the lower right corner. The dashed line is the 'FITEXY.pro' fit in the form of $\log y = \alpha + \beta \log x$. The values of α, β and Spearman's rank correlation coefficient $r_{\rm S}$ are shown in the figure.

and intervening between the central region and our eyes. At the present time, it is not clear whether or not photoionization models can reproduce the emission-line strengths other than Fe II under such a situation. Much broader exploration of photoionization model calculations is certainly needed.

4.2 Column density distribution inferred from Fe II(λ4570)/Fe II(UV)

Now we can roughly estimate column densities from the observed Fe II(λ4570)/Fe II(UV) by using equation (5). The estimated column density distribution is shown in Fig. 8. An average and a standard deviation of the distribution are found to be $(\overline{\log N_{\rm H}}, \sigma_{\log N_{\rm H}}) = (22.8, 0.5)$. Marconi et al. (2009) has suggested that radiation pressure does play an important role in BLR gas dynamics if column densities of BLR clouds have intrinsic dispersion such as $(\overline{\log N_{\rm H}}, \sigma_{\log N_{\rm H}}) = (23.0, 0.5)$. Our results support that the assumption adopted in Marconi et al. (2009) is appropriate and that the radiation pressure plays an important role in BLR clouds.

4.3 Correlation between the Eddington ratio and Fe II(λ4570)/Fe II(UV)

Fig. 9 shows the relation between Fe II(λ4570)/Fe II(UV) and the Eddington ratio. A positive correlation is seen. Linear regression analysis, using an IDL procedure 'FITEXY.pro' (cf. Press et al. 1992), gives the relation as

$$\log \frac{\text{Fe II}(\lambda 4570)}{\text{Fe II(UV)}} = -0.71 + 0.31 \log \frac{L_{\rm bol}}{L_{\rm Edd,0}}. \quad (16)$$

Spearman's rank correlation coefficient[3] for assessing the non-linear correlation is $r_{\rm S} = 0.58$. This means that the probability of the null hypothesis that there is no correlation is less than 10^{-13}. Thus, the correlation between Fe II(λ4570)/Fe II(UV) and the Eddington ratio is real. This implies that the column density increases with the Eddington ratio, because Fe II(λ4570)/Fe II(UV) increases with the column density.

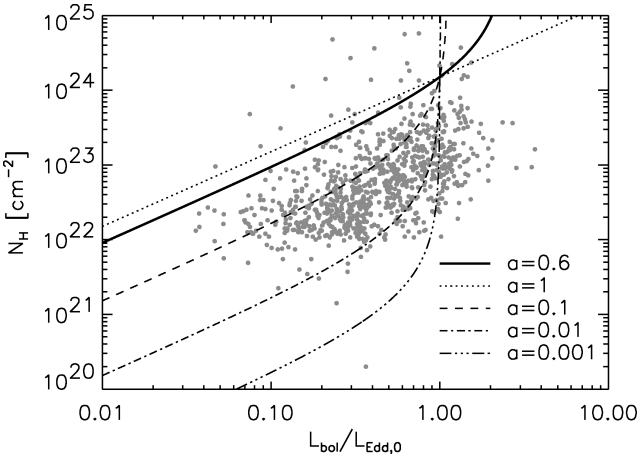

Figure 10. Estimated column densities versus $L_{\rm bol}/L_{\rm Edd,0}$. Each line represents $L_{\rm bol} = L_{\rm Edd,rad}$. Thick solid: $a = 0.6$ (adopted in Marconi et al. 2008), dotted: $a = 1$, dashed: $a = 0.1$, dot–dashed: $a = 0.01$ and dot–dot–dot–dashed: $a = 0.001$. Note that $a = L_{\rm ion}/L_{\rm bol}$. All these lines intersect at $N_{\rm H} = 1.5 \times 10^{24}\,{\rm cm}^{-2}$ and $L_{\rm bol}/L_{\rm Edd,0} = 1$, where $\sigma_{\rm T} N_{\rm H} = 1$.

As was recently suggested by Dong et al. (2009), under the condition where the BLR clouds are subject to the radiation pressure, low-column-density clouds would be blown away by relatively large radiation pressure at large $L_{\rm bol}/L_{\rm Edd,0}$, so that only high-column-density clouds would be able to be gravitationally bound. Fig. 9 is a supportive evidence for their suggestion.

4.4 Super-Eddington problem

Fig. 10 plots our samples on the $N_{\rm H}-L_{\rm bol}/L_{\rm Edd,0}$ plane. Each line represents $L_{\rm bol} = L_{\rm Edd,rad}$, so that the lower region of the line corresponds to a super-Eddington area. If we adopt ionizing photon fraction $a = 0.6$ (i.e. thick solid line in Fig. 10), which is an average value for AGNs calculated by Marconi et al. (2008), almost all of our samples become super-Eddington. This result can be interpreted in two ways: (i) the conversion from Fe II(λ4570)/Fe II(UV) to

[3] Spearman's rank correlation coefficient is a non-parametric measure of correlation, that is, which assesses how well an arbitrary monotonic function could describe the relationship between two variables without making any other assumptions

Downloaded from https://academic.oup.com/mnras/article/410/2/1018/1030498 by guest on 18 April 2024

column densities (i.e. equation 5) is wrong or (ii) the adopted value of a is inappropriate.

In case (i), since Fe II(λ4570)/Fe II(UV) is a function of the column density and the temperature, the failure in converting from the flux ratio to the column density is attributed to the assumed temperature. If we assume hot clouds such as $T_e > 10\,000$ K, the corresponding column densities would become large, resulting in a solution to this super-Eddington problem. However, as already discussed, the previous studies favour cold clouds such as $6000 < T_e < 10\,000$ K for Fe II emission (cf. Collin et al. 1980; Joly 1987). Thus, this interpretation seems to be inappropriate.

In case (ii), as can be seen from Fig. 10, if we adopt small values for a such as 0.01, the majority of our samples becomes gravitationally bound. This means that the fraction of ionizing photons irradiating on Fe II-emitting clouds is much less than that on usual BLR clouds. It then seems quite natural to conclude that the Fe II emission does not originate in the region where usual emission lines such as Hβ originate, but originate in outer parts of BLR where the incident ionizing photon fraction becomes as low as $a = 0.01$. It is worth noting that from the studies of O I and Ca II emission lines, Matsuoka, Kawara & Oyabu (2008) also suggest that Fe II emission originates in outer parts of BLR.

4.5 Eigenvector 1 in terms of the column density

Boroson & Green (1992) applied a principal component analysis to low-redshift quasars and found that the principal component 1 (which is called 'Eigenvector 1') links the strength of optical Fe II emission to the weakness of [O III] emission. After a while, Boroson (2002) showed that Eigenvector 1 is driven predominantly by an Eddington ratio. However, the physical causes making up Eigenvector 1 have been left unknown.

Here we propose a physical interpretation of Eigenvector 1 in terms of the column density. As discussed in the previous section, small-column-density clouds would be driven away from the line-emitting region by the radiation pressure at a large Eddington ratio, and only large-column-density clouds can be gravitationally bound. Radiative transfer effects make the optical Fe II emission become large in such large-column-density clouds. On the other hand, ionizing photons emitted from the central object are intervened by these large-column-density clouds and thus have less probabilities of ionizing photons reaching to NLR clouds, resulting in weak [O III] emission. In fact, fig. 10(t) in Tsuzuki et al. (2006) shows a negative correlation between the [O III]/Hβ and Fe II(O1)/Fe II(U1), which is almost the same as our Fe II(λ4570)/Fe II(UV), for 14 quasars.

5 SUMMARY

(i) Analysis of the Fe II(UV), Fe II(λ4570) and Mg II emission lines is performed for 884 SDSS quasars in a redshift range of $0.727 < z < 0.804$.

(ii) We suggest that Fe II(λ4570)/Fe II(UV) can be an indicator of the column density of Fe II-emitting clouds regardless of the excitation mechanism, i.e. photoionized or collisionally ionized clouds. From model calculations, we have confirmed this suggestion.

(iii) Our photoionization models underpredict Fe II(λ4570)/Fe II(UV) by a factor of 10, consistent with the preceding studies. Unless shocks are a viable heating mechanism, the failure of the photoionization model simply indicates that it is not predicting the correct heating rate or that the radiative transport calculations are not correct. Ignoring the anisotropy of UV Fe II emission may be one of the causes.

(iv) The column density distribution estimated from Fe II(λ4570)/Fe II(UV) is almost the same as the one suggested by Marconi et al. (2009), supporting that the radiation pressure does work on Fe II-emitting clouds.

(v) We also find a positive correlation between Fe II(λ4570)/Fe II(UV) and the Eddington ratio, implying the links between the column density and the Eddington ratio.

(vi) We find that under the assumption of the ionization fraction $a = 0.6$, almost all of our samples become super-Eddington. This problem can be cleared if the Fe II emission originates in outer parts of BLR where the ionizing photon fraction becomes as low as $a = 0.01$.

(vii) We propose physical interpretation of 'Eigenvector 1' in terms of the column density. In the interpretation, the strength of the optical Fe II emission results in the radiative transfer effects, while the weakness of the [O III] emission results in the reduction of ionizing photons in NLR caused by intervening large-column-density BLR clouds.

ACKNOWLEDGMENTS

We thank the anonymous referee for providing us with very helpful comments. This work was supported in part by Grant-in-Aid for JSPS Fellows, Scientific research (20001003), Specially Promoted Research on Innovative Areas (22111503), Research Activity Start-up (21840027) and Young Scientists (22684005).

REFERENCES

Baldwin J., Ferland G., Korista K., Verner D., 1995, ApJ, 455, L119
Baldwin J. A., Ferland G. J., Korista K. T., Hamann F., LaCluyzé A., 2004, ApJ, 615, 610
Boroson T. A., 2002, ApJ, 565, 78
Boroson T. A., Green R. F., 1992, ApJS, 80, 109
Collin S., Joly M., 2000, New Astron. Rev., 44, 531
Collin-Souffrin S., Joly M., Dumont S., Heidmann N., 1980, A&A, 83, 190
Dietrich M., Appenzeller I., Vestergaard M., Wagner S. J., 2002, ApJ, 564, 581
Dietrich M., Hamann F., Appenzeller I., Vestergaard M., 2003, ApJ, 596, 817
Dong X., Wang J., Wang T., Wang H., Fan X., Zhou H., Yuan W., 2009, preprint (arXiv:0903.5020)
Elston R., Thompson K. L., Hill G. J., 1994, Nat, 367, 250
Ferland G. J., Korista K. T., Verner D. A., Ferguson J. W., Kingdon J. B., Verner E. M., 1998, PASP, 110, 761
Ferland G. J., Hu C., Wang J. M., Baldwin J. A., Porter R. L., van Hoof P. A. M., Williams R. J. R., 2009, ApJ, 707, L82
Freudling W., Corbin M. R., Korista K. T., 2003, ApJ, 587, L67
Grandi S. A., 1982, ApJ, 255, 25
Hamann F., Ferland G., 1993, ApJ, 418, 11
Hu C., Wang J. M., Ho L. C., Chen Y. M., Zhang H. T., Bian W. H., Xue S. J., 2008, ApJ, 687, 78
Iwamuro F., Motohara K., Maihara T., Kimura M., Yoshii Y., Doi M., 2002, ApJ, 565, 631
Iwamuro F., Kimura M., Eto S., Maihara T., Motohara K., Yoshii Y., Doi M., 2004, ApJ, 614, 691
Joly M., 1987, A&A, 184, 33
Kaspi S., Smith P. S., Netzer H., Maoz D., Jannuzi B. T., Giveon U., 2000, ApJ, 533, 631
Kawara K., Murayama T., Taniguchi Y., Arimoto N., 1996, ApJ, 470, 85
Kuehn C. A., Baldwin J. A., Peterson B. M., Korista K. T., 2008, ApJ, 673, 69
Kurk J. D. et al., 2007, ApJ, 669, 32
McLure R. J., Jarvis M. J., 2002, MNRAS, 337, 109

Downloaded from https://academic.oup.com/mnras/article/410/2/1018/1030498 by guest on 18 April 2024

Maiolino R., Juarez Y., Mujica R., Nagar N. M., Oliva E., 2003, ApJ, 596, L155
Marconi A., Axon D. J., Maiolino R., Nagao T., Pastorini G., Pietrini P., Robinson A., Torricelli G., 2008, ApJ, 678, 693
Marconi A., Axon D. J., Maiolino R., Nagao T., Pietrini P., Risaliti G., Robinson A., Torricelli G., 2009, ApJ, 698, 103
Matsuoka Y., Oyabu S., Tsuzuki Y., Kawara K., 2007, ApJ, 663, 781
Matsuoka Y., Kawara K., Oyabu S., 2008, ApJ, 673, 62
Matteucci F., Panagia N., Pipino A., Mannucci F., Recchi S., Della Valle M., 2006, MNRAS, 372, 265
Nagao T., Murayama T., Taniguchi Y., 2001, ApJ, 546, 744
Netzer H., 2009, ApJ, 695, 793
Netzer H., Wills B. J., 1983, ApJ, 275, 445
Pei Y. C., 1992, ApJ, 395, 130
Press W. H., Teukolsky S. A., Vetterling W. T., Flannery B. P., 1992, Numerical Recipes. Cambridge Univ. Press, Cambridge
Sameshima H. et al., 2009, MNRAS, 395, 1087
Schlegel D. J., Finkbeiner D. P., Davis M., 1998, ApJ, 500, 525
Schneider D. P. et al., 2007, AJ, 134, 102
Totani T., Morokuma T., Oda T., Doi M., Yasuda N., 2008, PASJ, 60, 1327
Tsuzuki Y., Kawara K., Yoshii Y., Oyabu S., Tanabé T., Matsuoka Y., 2006, ApJ, 650, 57
Vanden Berk D. E. et al., 2001, AJ, 122, 549
Verner E. M., Verner D. A., Korista K. T., Ferguson J. W., Hamann F., Ferland G. J., 1999, ApJS, 120, 101
Verner E., Bruhweiler F., Verner D., Johansson S., Gull T., 2003, ApJ, 592, L59
Véron-Cetty M. P., Joly M., Véron P., 2004, A&A, 417, 515
Vestergaard M., Wilkes B. J., 2001, ApJS, 134, 1
Yoshii Y., Tsujimoto T., Nomoto K., 1996, ApJ, 462, 266
Yoshii Y., Tsujimoto T., Kawara K., 1998, ApJ, 507, 113

This paper has been typeset from a TEX/LATEX file prepared by the author.

Downloaded from https://academic.oup.com/mnras/article/410/2/1018/1030498 by guest on 18 April 2024